

Optical-fiber source of polarization-entangled photon pairs in the 1550 nm telecom band

Xiaoying Li, Paul L. Voss, Jay E. Sharping, and Prem Kumar*

Center for Photonic Communication and Computing, ECE Department

Northwestern University, Evanston, IL 60208-3118

(Dated: August 9, 2004)

Abstract

We present a fiber based source of polarization-entangled photon pairs that is well suited for quantum communication applications in the 1550 nm band of standard fiber-optic telecommunications. Polarization entanglement is created by pumping a nonlinear-fiber Sagnac interferometer with two time-delayed orthogonally-polarized pump pulses and subsequently removing the time distinguishability by passing the parametrically scattered signal and idler photon pairs through a piece of birefringent fiber. Coincidence detection of the signal and idler photons yields biphoton interference with visibility greater than 90%, while no interference is observed in direct detection of either the signal or the idler photons. All four Bell states can be prepared with our setup and we demonstrate violations of the CHSH form of Bell's inequality by up to 10 standard deviations of measurement uncertainty.

PACS numbers: 03.67.Hk, 42.50.Dv, 42.65.Lm

Quantum entanglement refers to the nonclassical interdependency of physically separable quantum subsystems. In addition to being at the heart of the most fundamental tests of quantum mechanics [1, 2, 3, 4], it is an essential resource that must be freely available for implementing many of the novel functions of quantum information processing [5, 6]. In photonic systems, the ongoing developments in lasers, optical-fiber technology, single-photon detectors, and nonlinear optical materials have led to enormous experimental progress in both the fundamental [7, 8, 9, 10, 11] and applied domains [12, 13, 14]. A popular approach to generating entangled pairs of photons is based on the nonlinear process of parametric down conversion in $\chi^{(2)}$ crystals [15, 16, 17]. Though much progress has been made using this approach, formidable engineering problems remain in coupling the entangled photons into standard optical fibers for transmission, storage, and manipulation over long distances.

The coupling problem can be obviated if the entangled photons can be generated in the fiber itself, and desirably, in the fiber's low-loss propagation window near $1.5\ \mu\text{m}$, since that would minimize losses during transmission as well. Apart from the inherent compatibility with the transmission medium, a fiber based source of entangled photons would have other advantages over its crystal counterparts [15, 16, 17, 18, 19, 20]. Particularly, the spatial mode of the photon-pair would be the guided transverse mode of the fiber, which is a very pure Gaussian-like single spatial mode in modern fibers. A well-defined mode is highly desirable for realizing complex networks involving several entangling operations. In this Letter, we describe the first, to the best of our knowledge, optical fiber source of polarization-entangled photon pairs in the 1550 nm telecom band. A variety of bi-photon interference experiments are presented that show the nature of the entanglement generated with this source. All four Bell states can be prepared with our setup and the CHSH form of Bell's inequality is violated by up to 10 standard deviations of measurement uncertainty.

Recently, our group has demonstrated that parametric fluorescence accompanying non-degenerate four-wave mixing (FWM) in standard optical fibers is an excellent source of quantum-correlated photon pairs [21]. The quantum correlation arises from four-photon scattering (FPS) events, wherein two pump photons at frequency ω_p scatter through the Kerr nonlinearity of the fiber to simultaneously create a signal photon and an idler photon at frequencies ω_s and ω_i , respectively, such that $\omega_s + \omega_i = 2\omega_p$. For a linearly polarized pump with wavelength close to the zero-dispersion wavelength of the fiber, the FWM process is phase-matched and the accompanying parametric fluorescence is predominantly co-polarized

with the pump. Since the response time of the Kerr nonlinearity is almost instantaneous, two such parametric scattering processes can be time and polarization multiplexed to create the desired polarization entanglement. For example [see Fig. 1(a)], when the fiber is pumped with two orthogonally polarized, relatively delayed pulses, the signal-idler photon pairs scattered from each pulse are co-polarized with that pump pulse and relatively delayed by the same amount. The distinguishing time delay between the orthogonally-polarized photon pairs, however, can be removed by passing the pairs through a piece of birefringent fiber of appropriate length, wherein the photon-pair travelling along the fast axis of the fiber catches up with the other pair travelling along the slow axis. When the emerging signal and idler photons are separated based on their wavelength, each stream of photons is completely unpolarized because any polarizer/detector combination is unable to determine which pump pulse a detected photon originated from. When the signal and idler photons are detected in coincidence, it is still impossible to determine which pump pulse created the detected pair. This indistinguishability gives rise to polarization entanglement in our experiment.

A schematic of the experimental setup is shown in Fig. 1(b). Signal and idler photon pairs at wavelengths of 1547.1 nm and 1525.1 nm, respectively, are produced in a nonlinear fiber Sagnac interferometer (NFSI) [21, 22]. The NFSI consists of a fused-silica 50/50 fiber coupler spliced to 300 m of dispersion-shifted fiber (DSF) that has a zero-dispersion wavelength at $\lambda_0 = 1535 \pm 2$ nm. Because the Kerr nonlinearity is weak, for this length of fiber only about 0.1 photon-pair is produced with a typical 5 ps-duration pump pulse containing $\sim 10^7$ photons. Thus, to reliably detect the correlated photon pairs, a pump-to-signal rejection ratio in excess of 100 dB is required. We achieve this by first exploiting the mirror-like property of the Sagnac loop, which provides a pump rejection of > 30 dB, and then sending the transmitted fluorescence photons along with the leaked pump photons through a free-space double-grating spectral filter (DGSF) that provides a pump rejection ratio in excess of 75 dB [21]. The filter consists of three identical diffraction gratings (holographic, 600 grooves/mm) G_2 , G_3 , and G_4 , whose diffraction efficiencies for the horizontally and the vertically polarized light are 90% and 86%, respectively. The doubly-diffracted signal and idler photons are then re-coupled into fibers, whose numerical apertures along with the geometrical settings of the gratings determine the pass bands for the signal and idler channels. The full-width at half-maximum (FWHM) bandwidth for both the channels is 0.6 nm.

During the experiment, for alignment and phase control purposes, input-signal and ref-

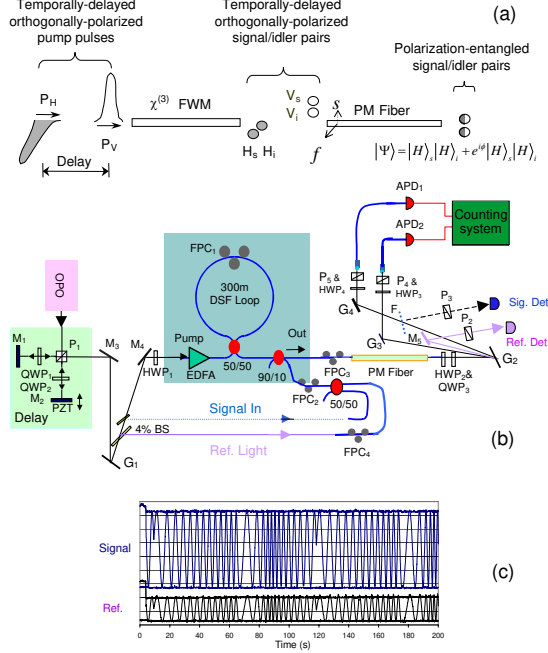


FIG. 1: (a) Conceptual representation of the multiplexing scheme used in our experiment to create polarization-entangled pairs of photons. (b) Schematic of the experimental setup. P_1 – P_5 , polarization beam splitters; G_1 – G_4 , diffraction gratings; M_1 – M_5 , mirrors; FPC_1 – FPC_4 , fiber polarization controllers; QWP, quarter-wave plate; HWP, half-wave plate; F, flipper mirror. (c) Sinusoidal variations (or constancy at the peaks and troughs) of the photocurrents obtained from the signal (top traces) and the reference detectors (bottom traces) upon linearly sweeping the voltage (or maintaining a fixed voltage) on the PZT. The clarity of the traces demonstrates minutes-long stability of the polarization interferometer formed between P_1 and P_3 (P_2) for signal (reference) light.

reference pulses are also needed that are temporally synchronized with the pump pulses. The main purpose of the signal pulses is to ensure that the time distinguishability between the orthogonally-polarized photon-pairs is effectively removed. By spectrally carving [22] the ~ 150 fs-pulse train from an optical parametric oscillator (Coherent Inc., model Mira-OPO), we obtain trains of 5-ps pump pulses with central wavelength at 1536 nm, 2.8-ps signal pulses with central wavelength at 1547 nm, and 4-ps reference pulses with central wavelength at 1539 nm. The pump pulses are then amplified by an erbium-doped fiber amplifier (EDFA) to achieve the required average pump power. Light at the signal and idler wavelengths from

the OPO that leaks through the spectral-carving optics and the amplified spontaneous emission from the EDFA are suppressed by passing the pump pulses through a 1 nm-bandwidth tunable optical filter (Newport, TBF-1550-1.0).

A 30-ps relative delay between the two orthogonally-polarized pump pulses is introduced by adding separate free-space propagation paths for the two pulses with use of a polarization beam splitter (PBS) P_1 , quarter wave-plates (QWP) QWP_1 and QWP_2 , and mirrors M_1 and M_2 . Mirror M_2 is mounted on a piezoelectric-transducer-(PZT)-driven translation stage, which allows precise adjustment of the relative delay and phase difference between the orthogonally-polarized pump-pulse pairs. After the NFSI, the delay is compensated by propagating the scattered photon pairs along the fast and slow polarization axes of 20 m-long polarization-maintaining (PM) fiber. A careful alignment procedure is implemented to properly orient the axes of the PM fiber, taking into consideration the change of polarization state incurred by an input signal-pulse pair upon maximally-amplified reflection from the NFSI [23]. Alignment is performed prior to the actual experiment by injecting weak path-matched signal-pulse pairs, having identical temporal and polarization structure as the pump pulses, into the NFSI through the 50/50 and 90/10 couplers. First the signal amplification is maximized by adjusting FPC_2 , while monitoring the signal gain on a detector (ETX500) placed after P_3 . Then the fringe visibility of the polarization interferometer formed between P_1 and P_3 is maximized by adjusting FPC_3 , HW_2 , and QWP_3 while observing the fringes in real time upon periodic scanning of M_2 . Once the alignment is completed, the injected signal is blocked and further measurements are made only on the parametric fluorescence.

After compensation of the time delay, the following polarization-entangled state is generated at the output of the PM fiber: $|\Psi\rangle = |H\rangle_s|H\rangle_i + e^{i\phi}|V\rangle_s|V\rangle_i$, where ϕ is the relative phase difference between the two-photon amplitudes $|H\rangle_s|H\rangle_i$ and $|V\rangle_s|V\rangle_i$. In our experiment $\phi = 2\phi_p$ with ϕ_p being the relative phase difference between the two delayed, orthogonally-polarized pump pulses. This source can produce all four polarization-entangled Bell states. When $\phi_p = 0, \frac{\pi}{2}$, the states $|\Psi^\pm\rangle = |H\rangle_s|H\rangle_i \pm |V\rangle_s|V\rangle_i$ are created. The other two Bell states $|\Phi^\pm\rangle = |H\rangle_s|V\rangle_i \pm |V\rangle_s|H\rangle_i$ can be prepared by inserting a properly oriented HWP in the idler channel. Non-maximally entangled pure states with an arbitrary degree of polarization entanglement can also be created with our setup by choosing the two pump pulses to have unequal powers.

In order to actively monitor and control the relative phase ϕ during the course of data

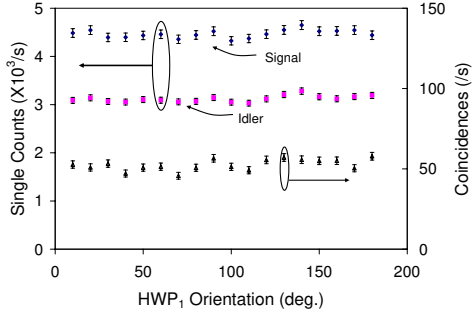


FIG. 2: Observed polarization (in)dependence of parametric fluorescence in the DSF.

taking, weak reference-pulse pairs of about $50 \mu\text{W}$ average power are injected into the NFSI through the 50/50 and 90/10 couplers. The reference-pulse pairs have identical temporal and polarization structure as the pump pulses, except the temporal location of the reference-pulse pairs is mismatched with respect to the pump-pulse pairs and their wavelength is slightly detuned, so that they neither interact with the pump pulses nor are seen by the single-photon detectors used in the signal and idler channels. During the course of measurements on the polarization-entangled states, the relative phase between the reference-pulse pairs, ϕ_{ref} , is monitored by measuring the photocurrent from a low-bandwidth reference detector placed after P_2 to make observations on one output port of the polarization interferometer [see Fig. 1(b)]. The voltage created by this photocurrent is compared to a reference voltage and the difference is used to stabilize ϕ_{ref} by feeding back on the PZT through an electronic circuit. The excellent overall stability of the system is shown by the near-perfect classical interference fringes displayed in the inset in Fig. 1(b), which were simultaneously obtained with injected signal light and with reference light while scanning ϕ_{ref} by ramping the voltage on the PZT. The relative phase between the reference-pulse pairs, ϕ_{ref} , is related to the relative phase between the pump-pulse pairs via $\phi_p = \phi_{\text{ref}} + \delta$, where δ results from dispersion in the DSF owing to slightly different wavelengths of the pulse pairs.

The photon-counting modules used for detecting the signal and idler photons consist of InGaAs/InP avalanche photodiodes (APDs, Epitaxx, EPM 239BA) operated in a gated-Geiger mode [21]. Gate pulses of 1-ns duration are applied at 588 kHz rate, 1/128 of the pump-pulse rate, to avoid after-pulsing in the detectors. The measured quantum efficiencies for the two detectors are 25% and 20%, respectively. The overall detection efficiencies for the signal and idler photons are about 9% and 7%, respectively, when the transmittance of

the Sagnac loop (82%), 90/10 coupler, DGSF (57%), and other optical components (90%) are included. Given a parametric scattering probability of $\simeq 0.1$ pairs/pulse in the DSF, corresponding to 0.39 mW of average pump power in each direction around the Sagnac loop, and the gate rate of 588 kHz, we typically observe $\simeq 4000$ counts/s in the signal and idler channels when detecting the parametric fluorescence.

The polarization-entanglement generation scheme described here uses the fact that the FPS efficiency does not depend on the pump-polarization direction. Moreover, the signal and idler fluorescence photons are predominantly co-polarized with the pump. Although the Kerr susceptibility tensor for isotropic fused-silica glass gives a cross-polarized scattering probability that is only 1/9th as strong, the actual scattering probability for cross-polarized fluorescence is even weaker owing to differing phase-matching condition for cross-polarized photons. We verify the polarization independence of the FPS efficiency in the fiber by monitoring the parametric fluorescence while varying the polarization direction of the injected pump pulses with use of a half-wave plate (HWP₁). The individual counts for the signal and idler photons, and their coincidence counts, versus the HWP₁ angle are shown in Fig. 2. The slight variation observed in the count rates is due to polarization-dependent transmission of the DGSF. Note that for the measurements shown in Fig. 2 the input pump delay, the PM-fiber delay compensation, and the detection analyzers were removed.

Polarization correlations are measured by inserting adjustable analyzers in the paths of signal and idler photons, each consisting of a PBS (P₄, P₅) preceded by an adjustable HWP (HWP₃, HWP₄). For the state $|\Phi\rangle = |H\rangle_s|V\rangle_i + e^{i\phi}|V\rangle_s|H\rangle_i$, when the relative phase between the down-converted pairs is ϕ and the polarization analyzers in the signal and idler channels are set to θ_1 and θ_2 , respectively, the single-count probability for the signal and idler photons is $R_i = \alpha_i/2$ ($i = 1, 2$) and the coincidence-count probability R_{12} is given by

$$R_{12} = 2^{-1}\alpha_1\alpha_2[\sin^2\theta_1\cos^2\theta_2 + \cos^2\theta_1\sin^2\theta_2 + 2\cos\phi\sin\theta_1\cos\theta_1\sin\theta_2\cos\theta_2], \quad (1)$$

where α_i is the total detection efficiency in the two channels.

We performed three sets of experiments to evaluate the degree of polarization entanglement of our source. The first measurement consisted of setting both analyzers at 45° and slowly scanning ϕ_{ref} by applying a voltage ramp on the PZT. As shown in Fig. 3(a), the coincidence counts reveal sinusoidal variation with a fringe visibility of 93% (dark counts

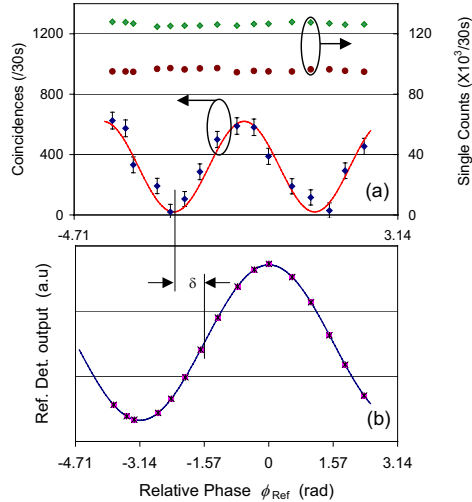


FIG. 3: (a) Coincidence counts and single counts detected over 30 s when the relative phase ϕ_{ref} is varied. The solid curve a fit to Eq. 1. (b) Output from the reference detector versus ϕ_{ref} showing the ordinary one-photon interference with twice the fringe spacing as in (a).

and accidental-coincidence counts have been subtracted), while the single counts remain unchanged. The output from the reference detector is also recorded simultaneously, which is shown in Fig. 3(b). The relative shift of the sinusoidal variation of two-photon interference in Fig. 3(a) from that of reference-light interference in Fig. 3(b) is a direct measure of the phase shift δ , which is used below to properly set ϕ for measurements of the violation of Bell's inequality.

In the second set of measurements on polarization entanglement, we locked the generated state to $|\Phi^-\rangle = |H\rangle_s|V\rangle_i - |V\rangle_s|H\rangle_i$ by applying an appropriate feedback on the PZT, fixed the angle of the polarization analyzer in the signal channel to 45° , and varied the analyzer angle in the idler channel by rotating HWP₄. The result is shown in Fig. 4. As expected, the coincidence-count rate displays sinusoidal interference fringes with a visibility of 92%, whereas the variation in the single-count rate is only 4% (once again, dark counts and accidental coincidences have been subtracted).

In the third set of experiments, we characterized the quality of polarization entanglement produced with our source through measurements of Bell's inequality violation. By recording coincidence counts for 16 different combinations of analyzer settings with $\theta_1 = 0^\circ, 90^\circ, -45^\circ, 45^\circ$ and $\theta_2 = -22.5^\circ, 67.5^\circ, 22.5^\circ, 112.5^\circ$, we measured the quantity S in the CHSH form of Bell's inequality [3], which satisfies $|S| \leq 2$ for any local realistic descrip-

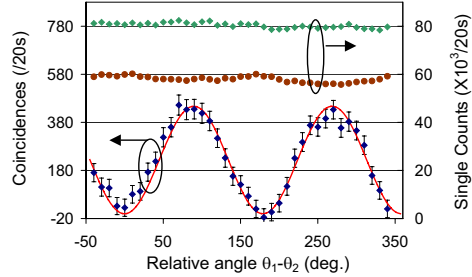


FIG. 4: Measurement of polarization entanglement: Coincidence counts and single counts detected over 20 s as the analyzer angle in the idler channel is varied while keeping the signal-channel analyzer fixed at 45° relative to vertical.

TABLE I: Measured values of S for the four Bell states.

Bell state	S	Violation (standard deviations)
$ H\rangle_s H\rangle_i + V\rangle_s V\rangle_i$	2.75 ± 0.077	10σ
$ H\rangle_s H\rangle_i - V\rangle_s V\rangle_i$	2.55 ± 0.070	8σ
$ H\rangle_s V\rangle_i + V\rangle_s H\rangle_i$	2.48 ± 0.078	6σ
$ H\rangle_s V\rangle_i - V\rangle_s H\rangle_i$	2.64 ± 0.076	8σ

tion of our experiment. The results, which are presented in Table I, show that a) the CHSH inequality is violated, i.e., $|S| > 2$, for all four Bell states produced with our setup and b) the violation occurs by up to 10 standard deviations of measurement uncertainty.

In order to ascertain the degree of entanglement produced by the true FPS events in our setup, the accidental coincidences resulting from the uncorrelated background photons and the dark counts in the detectors were measured for each set of data acquired in the three polarization-entanglement experiments described above. The rate of accidental coincidences was as large as the rate of “true” coincidences plotted in Figs. 2–4 by subtracting the accidental coincidences and the raw visibility of two-photon interference was only $\simeq 30\%$. We believe the majority of background photons in our setup arise from spontaneous Raman scattering [24, 25]. Our recent measurements with a modified DGSF have shown that the contribution of accidental coincidences can be made $< 10\%$ of the total measured coincidences [26]. With these improvements, a raw two-photon-interference visibility of $> 85\%$

would be obtained, i.e., without any post-measurement corrections.

In conclusion, we have developed and characterized a fiber-based source of polarization-entangled photon pairs. The count rates in the experiment at present are limited by the repetition rate of the APDs, which can be increased by at least an order of magnitude by straightforward refinements of the detection electronics. The photon-pair production rate, on the other hand, is limited by the 75 MHz repetition rate of the pump laser. The production rate can be dramatically increased by using state-of-the-art pulsed lasers that have been developed for fiber-optic communications. These lasers operate at 10–40 GHz repetition rates and can have the requisite peak-pulse powers with use of medium-power EDFAs. Bulk-optic implementations of the pump delay apparatus and the detection filters were used in these proof-of-principle experiments for purposes of tunability and control. All-fiber versions of these subsystems can be readily realized with use of PM fibers, wavelength-division-multiplexing filters, and fiber polarizers. Finally, we have understood the origin of the large number of accidental coincidences in the experiment and subsequent system improvements are expected to significantly improve the degree of entanglement produced with our system. Therefore, we believe that such fiber-based entangled-photon pairs will prove to be an efficient source for developing quantum communication technologies.

This work was supported in part by the DoD Multidisciplinary University Research Initiative (MURI) Program administered by the Army Research Office under Grant DAAD19-00-1-0177.

* xyli@ece.northwestern.edu

- [1] A. Einstein, B. Podolsky, and N. Rosen, *Phys. Rev.* **47**, 777 (1935).
- [2] J. S. Bell, *Physics* **1**, 195 (1964).
- [3] J. F. Clauser, M. A. Horne, A. Shimony, and R. A. Holt, *Phys. Rev. Lett.* **23**, 880 (1969).
- [4] D. M. Greenberger, M. A. Horne, A. Shimony, and A. Zeilinger, *Am. J. Phys.* **58**, 1131 (1990).
- [5] C.H.Bennett and S. J. Wiesner, *Phys. Rev. Lett.* **69**, 2881 (1992).
- [6] C. H. Bennett, G. Brassard, C. Crèpeau, R. Jozsa, A. Peres, and W. K. Wootters, *Phys. Rev. Lett.* **70**, 1895 (1993).
- [7] A. Aspect, P. Grangier, and G. Roger, *Phys. Rev. Lett.* **49**, 91 (1982).

- [8] Z. Y. Ou and L. Mandel, Phys. Rev. Lett. **61**, 50 (1988).
- [9] Z. Y. Ou, L. J. Wang, X. Y. Zou, and L. Mandel, Phys. Rev. A **41**, 566 (1990).
- [10] Y. H. Shih and C. O. Alley, Phys. Rev. Lett. **61**, 2921 (1988).
- [11] J. W. Pan, D. Bouwmeester, M. Daniell, H. Weinfurter, and A. Zeilinger, Nature **403**, 515 (2000).
- [12] K. Mattle, H. Weinfurter, P. G. Kwiat, and A. Zeilinger Phys. Rev. Lett **76**, 4656 (1996).
- [13] D. Bouwmeester, J. W. Pan, K. Mattle, M. Eibl, H. Weinfurter, and A. Zeilinger, Nature **390**, 575 (1997).
- [14] N. Gisin, G. Ribordy, W. Tittel, and H. Zbinden, Rev. Mod. Phys. **74**, 145 (2002).
- [15] P. G. Kwiat, K. Mattle, H. Weinfurter, A. Zeilinger, A. V. Sergienko, and Y. Shih, Phys. Rev. Lett. **75**, 4337 (1995).
- [16] J. G. Rarity and P. R. Tapster, Phys. Rev. Lett. **64**, 2495 (1990).
- [17] J. Brendel, E. Mohler, and W. Martienssen, Europhys. Lett. **20**, 575 (1992).
- [18] K. Sanaka, K. Kawahara, and T. Kuga, Phys. Rev. Lett. **86**, 5620 (2001).
- [19] J. Kim, O. Benson, H. Kan, and Y. Yamamoto, Nature **397**, 500 (1999).
- [20] C. Kurtsiefer, S. Mayer, P. Zarda, and H. Weinfurter, Phys. Rev. Lett. **85**, 290 (2000).
- [21] M. Fiorentino, P. Voss, J. E. Sharping, and P. Kumar, IEEE Photon. Technol. Lett. **14**, 983 (2002).
- [22] J. E. Sharping, M. Fiorentino, and P. Kumar, Opt. Lett. **26**, 367 (2001).
- [23] D. B. Mortimore, J. Lightwave Tech. **6**, 1217 (1988).
- [24] P. L. Voss and P. Kumar, Opt. Lett. **29**, 445 (2004).
- [25] P. L. Voss and P. Kumar, to appear in J. Opt. B: Quantum Semiclass. Opt. **6** (2004).
- [26] X. Li, J. Chen, P. L. Voss, J. E. Sharping, and P. Kumar, Opt. Express. **12**, 3337 (2004).